Photoionization of $[Ru(bpy)_3]^{2+}$: A Catalytic Cycle with Water as Sacrificial Donor

Martin Goez,* Daniel von Ramin-Marro, Mohammad Hussein Othman Musa, and Martin Schiewek

Fachbereich Chemie, Martin-Luther-Universität Halle-Wittenberg, Kurt-Mothes-Strasse 2, D-06120 Halle/Saale, Germany

Received: September 18, 2003; In Final Form: November 21, 2003

The photoionization of the tris-2,2′-bipyridyl ruthenium(II) ion $[Ru(bpy)_3]^{2+}$ in water was investigated by laser-flash photolysis at 308, 355, and 532 nm up to very high excitation intensities I_{exc} (500. . .900 mJ/cm^2). By single-pulse absorption and two-pulse luminescence measurements, it was established that the mechanism is cyclic and comprises three steps: excitation of $[Ru(bpy)_3]^{2+}$ to the metal-to-ligand charge-transfer (MLCT) excited state $*[Ru(bpy)_3]^{2+}$, ionization of $*[Ru(bpy)_3]^{2+}$ by a second photon to give a hydrated electron $e_{aq}^{\bullet-}$ and the oxidized complex $[Ru(bpy)_3]^{3+}$, and photoreduction of $[Ru(bpy)_3]^{3+}$ by water. No other species is involved in the reaction. Experiments on chemically generated $[Ru(bpy)_3]^{3+}$ yield direct evidence for the photoreduction step and show that it is completed in less than 30 ns. The concentrations of $[Ru(bpy)_3]^{2+}$, $*[Ru(bpy)_3]^{2+}$, $[Ru(bpy)_3]^{3+}$, and $e_{aq}^{\bullet-}$ at the end of the laser pulse were measured as functions of I_{exc}. Closed-form expressions for these dependences were derived by a kinetic treatment. Very good simultaneous fits to the concentrations of all species were obtained with three global kinetic parameters only. A decision as to whether the photoreduction leads back to $[Ru(bpy)_3]^{2+}$ or to $*[Ru(bpy)_3]^{2+}$ is kinetically impossible in that system, but evidence pointing to a delayed generation of $*[Ru(bpy)_3]^{2+}$ by this reaction step is presented, which would also explain short-time anomalies of the luminescence reported in the literature. The quantum yield ϕ_2 of the photoionization step is the same at 308 and 355 nm, is independent of pH, and is an order of magnitude higher (0.016 ± 0.001) than previously thought. The quantum yield ϕ_3 of the photoreduction is comparable to ϕ_2 at pH 7 but lower by a factor of 14 at pH 0.

Introduction

Photochemistry at high light intensities is a compelling subject because the absorption of more than one photon opens up new reaction pathways,[1] for instance, catalytic cycles of photoionization in the visible or near-UV range.[2−4]

As we recently found, such photoionizations can be greatly facilitated by a preceding charge separation.[2,5] The irradiation of an acceptor A in the presence of a sacrificial donor D_{sac} provides the simplest case (Scheme 1): photoinduced electron transfer produces the radical anion $A^{\bullet-}$, from which the unpaired electron can be easily ejected by another photon because this regenerates A (i.e., leads to a stable molecule).

SCHEME 1

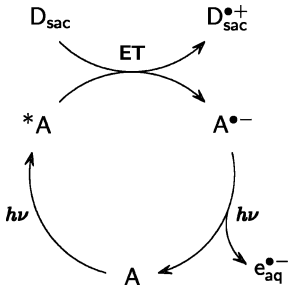

The intermediacy of an excited state *A in the photoinduced electron transfer can be disregarded only for low light levels, long unquenched lifetimes of *A, and/or high quencher concentrations; otherwise, the number of hydrated electrons $e_{aq}^{\bullet-}$ formed in a given time is limited by the rate and efficiency of the quenching of *A by D_{sac}. These restrictions are largely absent when the charge transfer is intramolecular. There are several ways in which a sacrificial donor might interact with such a system. The two mechanisms that utilize D_{sac} to reduce the

SCHEME 2

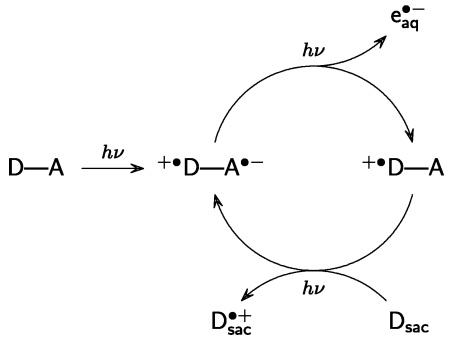

SCHEME 3

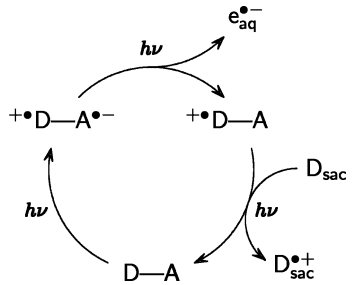

* Author to whom correspondence should be addressed. E-mail: goez@chemie.uni-halle.de.

10.1021/jp036790r CCC: $27.50
Published on Web 01/14/2004

oxidized form $^{+\bullet}$D−A of a donor−acceptor molecule D−A are shown in Schemes 2 and 3. Because ions usually live longer than do excited states, these variants possess advantages over those where the function of the sacrificial donor is to quench the charge-separated excited state $*(^{+\bullet}D-A^{\bullet-})$.

Inorganic examples of such donor−acceptor systems are provided by transition-metal complexes with metal-to-ligand charge-transfer (MLCT) excited states, their most popular representative being the tris-2,2′-bipyridyl ruthenium(II) ion $[Ru(bpy)_3]^{2+}$: the MLCT state of that complex is best described as $[Ru^{III}(bpy^{\bullet-})(bpy)_2]^{2+}$, with the electron located on one of the three bpy ligands only.[6] Our second motive for investigating the photoionization of that compound was that it might constitute a "minimum version" of photochemical water cleavage because $e_{aq}^{\bullet-}$ produces hydrogen from water[7] and the oxidized complex $[Ru(bpy)_3]^{3+}$ is thermodynamically capable of oxidizing water to oxygen.[8] This opens up the intriguing possibility of water acting as the sacrificial donor in the catalytic cycles of Scheme 2 or 3.

SCHEME 4

$$[Ru(bpy)_3]^{2+} \xrightarrow{h\nu} *[Ru(bpy)_3]^{2+} \xrightarrow{h\nu} [Ru(bpy)_3]^{3+} + e_{aq}^{\bullet-}$$

Despite strong interest in the photophysics and photochemistry of $[Ru(bpy)_3]^{2+}$,[8,9] especially with a view toward solar-energy harvesting, its photoionization has received little attention so far. Meisel et al. proposed a biphotonic ionization according to Scheme 4 on the basis of flash-lamp photolysis with polychromatic light (300−360 nm, 17-μs pulse length) in which $e_{aq}^{\bullet-}$ was not observed directly;[10] a very low quantum yield of photoionization (0.0015) was inferred from these experiments. Three later studies using nanosecond laser-flash photolysis at 355 nm and the optical detection of $e_{aq}^{\bullet-}$ gave no other mechanistic interpretation and were predominantly[11,12a] or even exclusively[12b] concerned with the increase in the electron yield when the surfactant sodium dodecyl sulfate SDS was added.

In a recent communication,[3] we have presented initial evidence that the photoionization of $[Ru(bpy)_3]^{2+}$ is a catalytic cycle rather than a sequential two-photon ionization. The step closing the cycle is a hitherto unrecognized photoreduction of the oxidized complex that involves water as a sacrificial donor. In this work, we have undertaken a detailed mechanistic study of the reaction that corroborates the preliminary findings. We have used complementary detection techniques, in particular, single-pulse absorption and two-pulse luminescence measurements, and have monitored the absolute concentrations of all species participating in the reaction. The advantages of such an approach for the elucidation of a complex mechanism are obvious. As we will show, these experiments give a consistent picture of the reaction and lead to a reappraisal of the photoionization efficiency[10] and of reported short-time effects in the luminescence spectra that were ascribed to ligand-field excited dd states as intermediates.[13]

Experimental Section

The laser-flash photolysis setup has been described in ref 2b. It is optimized for the homogeneous illumination of the detection volume at very high excitation intensities. The optical path length for detection is 0.4 cm; the other two dimensions of the active volume are 0.2 cm each. Both absorption and luminescence can be used for detection.

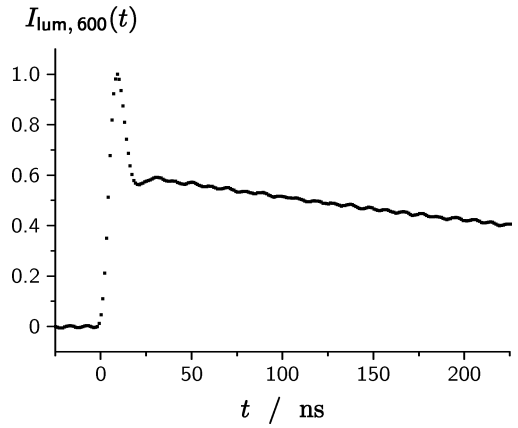

Figure 1. Early part of the normalized luminescence decay $I_{lum,600}(t)$ at 600 nm of a sample of 3×10^{-5} M $[Ru(bpy)_3]^{2+}$ excited at 355 nm, with an excitation intensity of 531 mJ/cm^2.

To increase the signal-to-noise ratio, between 10 and 100 acquisitions were averaged per measurement. A flow-through system was used to ensure that each laser flash hits fresh solution. Oxygen was removed by purging the solutions with argon or with N_2O.

All chemicals were obtained commercially in the highest available purity and used without further purification. The solvent was ultrapure Millipore MilliQ water (resistance 18.2 MΩ cm^{-1}). To all solutions, 0.5 M *tert*-butyl alcohol was added to scavenge the $^{\bullet}$OH radicals formed from N_2O and $e_{aq}^{\bullet-}$. The concentration of $[Ru(bpy)_3]^{2+}$ was 3×10^{-5} M throughout. At that concentration, inner filter effects were found to be absent.

$[Ru(bpy)_3]^{3+}$ was prepared in situ by the oxidation of $[Ru(bpy)_3]^{2+}$ with lead(IV) dioxide or cerium(IV),[14] a slight excess of the oxidant over the stoichiometric amount being employed, and in acidic solution (pH 0), where it is sufficiently stable for our measurements.

The extinction coefficient of $e_{aq}^{\bullet-}$ was measured relative to the maximum by a difference experiment such as the one shown in Figure 4; the maximum value was taken from ref 7.

Results and Discussion

Short-Time Behavior of the MLCT Transient Signals. In a recent paper,[13] short-time anomalies of the MLCT emission and absorption at high excitation intensities, namely, an additional rising component with a time constant of 27 ns, were reported and attributed to the involvement of ligand-field excited dd states. This prompted us to check whether such effects might play a significant role in the evaluation of our measurements and the interpretation of the results, especially because the excitation conditions (laser wavelength, intensity, and duration) of our experiments appeared to be similar to those of that work.

However, we were not able to reproduce those observations convincingly. Figure 1 shows the transient emission at the luminescence maximum for the highest excitation intensity available on our laser-flash spectrometer, which falls within 5% of the intensity used in ref 13.

At early times, the luminescence signal overshoots considerably. The absence of any such signal when solutions not containing $[Ru(bpy)_3]^{2+}$ are employed rules out both stray light and impurities in the reaction medium as the reason. Luminescence spectra acquired at the maximum of the peak and 50 ns afterward do not differ, which excludes a contamination of the substrate. The low concentration used (3×10^{-5} M) eliminates triplet−triplet annihilation as the origin of the phenomenon. We would ascribe the effect to an artifact of our electronic system

were it not for the fact that the peak seems to follow closely the envelope of the laser pulse and exhibits hardly any negative overshoot after the pulse end.

We cannot completely rule out that what we tend to regard as the tail of the overshoot ring-down, from 20 to 30 ns in the Figure, is a rising component of the luminescence instead or that at early times such a component is obliterated by the superimposed peak. However, no rising component is discernible at times later than 30 ns after the start of the pulse, which is ca. 20 ns after its end, and it can be seen that both the time resolution and the signal-to-noise ratio would have permitted the detection of a 27-ns component with a relative amplitude as large as that reported in ref 13. Hence, if such a component exists, then its amplitude must be considerably smaller and its time constant considerably shorter in our experiments. Absorption measurements gave the same result.

Our setup is optimized for homogeneous excitation, whereas the description in ref 13 seems to indicate that the laser was focused into the sample. In that case, nonlinear absorption might be the reason for the reported effect and might well cause dd states to be reached. Because we can find no hard evidence for their involvement under our experimental conditions but will present below an alternative explanation of a possible luminescence rise after the pulse end and because their presence or absence does not affect any of the other results and conclusions of this paper, we will, by the principle of Occam's razor, not include them in the reaction mechanism.

At all excitation intensities, we found clear monoexponential decays after the initial perturbation over a range of at least 98% of the luminescence and absorption signals (in the case of the latter after having removed, if necessary, a constant residual absorption by the procedure described below). Therefore, to get accurate initial amplitudes, we fitted each decay curve for about one time constant τ, starting some 50 ns after the end of the laser pulse, and extrapolated the fitted curve back to the pulse end. The small extrapolation range (less than 10% of τ) and the strictly monoexponential behavior make the extrapolation very reliable. This approach avoids errors arising from the distortion of the early part of the decay curves, regardless of what their true origin is (dd states or instrumental artifacts), and from the fact that the two lasers that were used have different pulse widths (532 and 355 nm, ca. 8 ns; 308 nm, ca. 30 ns).

Excitation at 532 nm. Reports[15,16] of an irreversible decomposition of $[Ru(bpy)_3]^{2+}$ upon irradiation into the MLCT band caused us to investigate the stability of this compound at 532 nm up to very high excitation intensities. However, we found no evidence of any photochemistry under these conditions, neither on short nor on long time scales:

The excitation of $[Ru(bpy)_3]^{2+}$ by light of wavelength 532 nm leads to the formation of the MLCT state $*[Ru(bpy)_3]^{2+}$ with its characteristic luminescence. The transient luminescence is accompanied by a transient absorption. Neither the luminescence spectrum nor the absorption spectrum changed when we increased the excitation intensity I_{exc} up to about 900 mJ/cm^2, which excludes the formation of another transient at high I_{exc}. There was also no significant influence on the excited-state lifetime τ, which is about 620 ns at low I_{exc}; at the highest intensity, τ was shortened by less than 8%.

As long as the only process that occurs is the decay of the MLCT state to regain the ground state (subscript GS), the transient absorption signal, $\Delta E_\lambda(I_{exc}, t)$, must be given by

$$\Delta E_\lambda(I_{exc}, t) = \Delta\epsilon_{MLCT,\lambda} \cdot c_{MLCT}(I_{exc}, t) \cdot d \qquad (1)$$

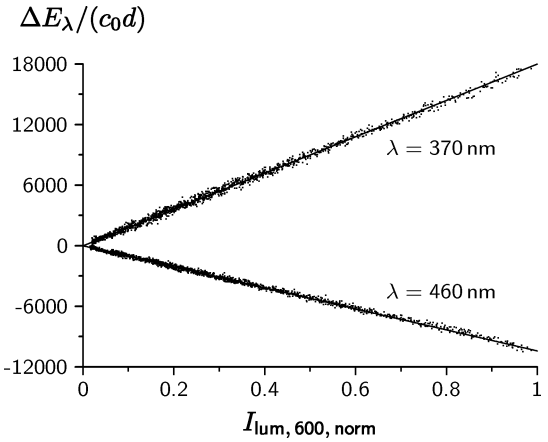

Figure 2. Transient absorptions ΔE_λ at wavelengths λ (given at the traces) divided by the starting concentration c_0 and the optical path length d as functions of the transient luminescence at 600 nm of the same sample acquired under identical conditions, $I_{lum,600,norm}$, which was normalized to the limiting value at extremely high excitation intensities (cf. Figure 3). The data stem from a superposition of several pairs of decay traces. Conditions: $c_0 = 3 \times 10^{-5}$ M $[Ru(bpy)_3]^{2+}$, excitation wavelength 532 nm, excitation intensity between 13 and 460 mJ/cm^2. At $I_{lum,600,norm} = 1$, the value of each regression line directly gives the respective difference extinction coefficient, $\Delta\epsilon_{MLCT,\lambda} = (\epsilon_{MLCT,\lambda} - \epsilon_{GS,\lambda})$.

with

$$\Delta\epsilon_{MLCT,\,\lambda} = \epsilon_{MLCT,\,\lambda} - \epsilon_{GS,\,\lambda} \qquad (2)$$

whereas any formation of longer-lived photoproducts would reveal itself by an absorption remaining after the MLCT state has disappeared. No such residual signals were found at any observation wavelength when 532-nm excitation was used.

If the MLCT state is the only luminescent species in this system, then the luminescence signal $I_{lum,\lambda'}(I_{exc}, t)$ is related to the concentration of the MLCT state by

$$I_{lum,\,\lambda'}(I_{exc}, t) = f_{\lambda'} \cdot c_{MLCT}(I_{exc}, t) \qquad (3)$$

where the factor $f_{\lambda'}$ comprises substrate-specific (e.g., luminescence quantum yield) and instrument-specific (e.g., detector sensitivity) parameters. Equations 1 and 3 demand a direct proportionality between the transient emission and absorption signals, whereas more complex deactivation mechanisms of $*[Ru(bpy)_3]^{2+}$, including pathways that do not lead to permanent products and thus possibly not to residual absorptions, would cause deviations from this strict proportionality. We found no evidence whatsoever for such deviations; for the two characteristic wavelengths of 370 and 460 nm, corresponding to the long-wavelength maxima of the MLCT and the ground-state absorption, respectively, the pertinent plots are shown in Figure 2.

Last, we did not observe any changes in the luminescence spectrum or a decrease in the luminescence intensity when we stopped the flow and acquired the luminescence after having irradiated the same volume with 100 flashes of intensity 900 mJ/cm^2 each. Hence, we have to conclude that there is no photochemical decomposition of $[Ru(bpy)_3]^{2+}$ (or $*[Ru(bpy)_3]^{2+}$) at 532 nm under our experimental conditions. The longer excitation wavelength in our experiments is the most probable reason for the discrepancy between our results and those reported: the absorption spectrum of $[Ru(bpy)_3]^{2+}$ exhibits a distinct shoulder at about 420 nm, so different photochemistry upon excitation at 436 nm, as in the references cited, and at 532 nm, as in our work, is no contradiction.

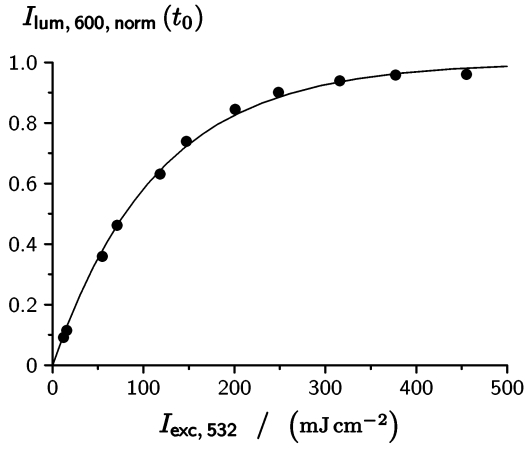

Figure 3. Dependence on the excitation intensity $I_{exc,532}$ of the initial values of the transient luminescence at 600 nm, $I_{lum,600,norm}$ (t_0), normalized to the limiting value at infinite $I_{exc,532}$. Conditions: 3×10^{-5} M $[Ru(bpy)_3]^{2+}$, excitation wavelength 532 nm. Fit curve $1 - \exp(-\kappa_1 I_{exc,532})$; best-fit parameter $\kappa_1 = 8.7 \times 10^{-3}$ cm²/mJ.

Figure 3 displays the dependence of the initial luminescence signal on the excitation intensity $I_{exc,532}$. It is seen that the conversion of $[Ru(bpy)_3]^{2+}$ to $*[Ru(bpy)_3]^{2+}$ is already complete at about 400 mJ/cm² (i.e., less than 50% of our maximum available $I_{exc,532}$). From the limiting value of the curve shown in Figure 3, the factor $f_{\lambda'}$ (cf. eq 3) can be obtained, which relates the absolute concentration of the MLCT state to the luminescence signal. A high-intensity 532-nm pulse can thus be used to probe quantitatively the concentration of the ground state or to establish an arbitrary concentration ratio of $[Ru(bpy)_3]^{2+}$ and $*[Ru(bpy)_3]^{2+}$ as a starting condition for a photoreaction induced by a second laser pulse.

Analogous curves are found for the transient absorptions and yield $\Delta\epsilon_{MLCT,\lambda}$ at an observation wavelength λ; this difference in extinction coefficients is obtained most reliably from plots as shown in Figure 2. The spectrum of the MLCT state is given below (Figure 9).

Excitation in the UV. Irradiation with 355- or 308-nm light leads to photochemistry, as evidenced by the formation of hydrated electrons $e_{aq}^{\bullet-}$.[3,10−12] The concentration of $e_{aq}^{\bullet-}$ is conveniently determined by its optical absorption. At its absorption maximum around 720 nm, the measurements are disturbed by the luminescence of the MLCT state, which is still noticeable at that wavelength. To avoid this source of errors, we observed the electrons further into the red, at 830 nm.[17] As a second complication, the MLCT state also absorbs in this range.[18] To eliminate this problem, which is especially severe at low to medium excitation intensities, we performed difference experiments: Each series of intensity-dependent measurements was first carried out in an argon-saturated solution and then immediately repeated with the solution saturated with N_2O; from two such measurements without and with N_2O but with all other experimental parameters being identical, the pure electron absorption is obtained as the difference in the traces. Figure 4 shows that the omission of this procedure would lead to gross errors.

In an N_2O-saturated solution, the electron lifetime is reduced to about 6 ns,[7] which means that a determination of the electron concentration at the end of the laser pulse by the described fitting procedure is feasible; because we found typical electron lifetimes of around 450 ns, the extrapolation is again quite reliable. From the observation that N_2O saturation has no significant effect on the intensity dependence and decay of the MLCT luminescence, we conclude that it works as a specific electron scavenger in our system and does not affect the photoreaction in any other way. We stress that, throughout this paper, N_2O saturation was used when species other than the electron were monitored in photoionization experiments; hence, reactions of $e_{aq}^{\bullet-}$ with any ruthenium-based species can be generally disregarded.

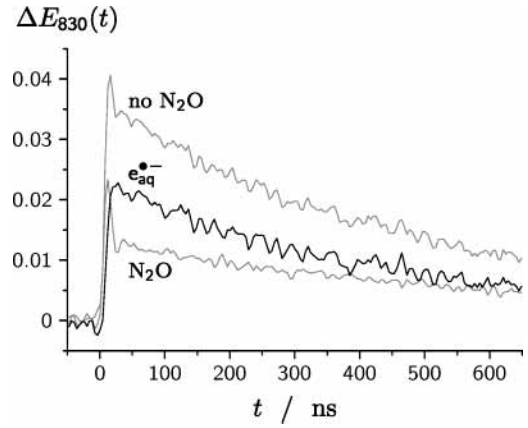

Figure 4. Monitoring the hydrated electron $e_{aq}^{\bullet-}$ by measurements of the transient absorptions $\Delta E_{830}(t)$ at 830 nm. The traces marked "no N_2O" and "N_2O" were recorded in argon-saturated and N_2O-saturated solutions, respectively; their subtraction yields the transient absorption of $e_{aq}^{\bullet-}$. Experimental parameters: 3×10^{-5} M $[Ru(bpy)_3]^{2+}$, excitation wavelength 355 nm, excitation intensity 129 mJ/cm².

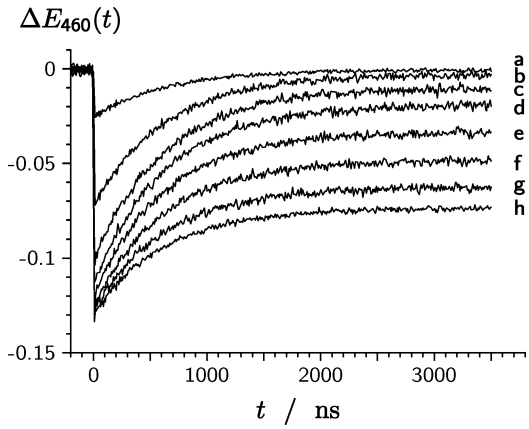

Figure 5. Transient absorptions $\Delta E_{460}(t)$ at 460 nm of an N_2O-saturated solution of 3×10^{-5} M $[Ru(bpy)_3]^{2+}$, with an excitation wavelength of 355 nm. The excitation intensity increases monotonically from trace a (ca. 6 mJ/cm²) to trace h (ca. 500 mJ/cm²).

When excitation with 308- or 355-nm light is used, the dependence of the luminescence amplitude on I_{exc} no longer exhibits a simple saturation behavior as in Figure 3 but passes through a maximum at intermediate I_{exc}; the ensuing decrease is steeper for 355-nm excitation than for 308-nm excitation (cf. Figures 8 and 11 below). However, both the luminescence spectrum and the luminescence lifetime remain unchanged when I_{exc} or the excitation wavelength is varied. This bears out that the MLCT state is the only emitting species also under these excitation conditions.

Likewise, the transient absorptions show a more complex behavior. They do not fall back to zero at high I_{exc} but to a residual absorption, which is positive or negative, depending on λ. There is a manifestly dissimilar dependence on I_{exc} of the magnitude of this residual absorption and that of the initial—again, positive or negative—rise of the transient absorption. A few representative traces acquired at 460 nm are displayed in Figure 5.

To remove the absorption signals of $e_{aq}^{\bullet-}$, these measurements were carried out in N_2O-saturated solutions. Subtract-

ing the residual absorption remaining at long times yields the pure decay. In all cases, this was found to be monoexponential. The decay time agreed extremely well with that of a luminescence trace acquired under identical conditions, and in a series of runs with varying I_{exc} but all other parameters kept constant, the amplitudes of the exponentials in the corresponding absorption and emission traces were proportional. This suggests that the time dependence of the transient absorption solely reflects the deactivation of the MLCT state whereas the constant residual absorption is due to the formation of one or several products that are stable on a time scale of at least 10 μs.

If the limiting absorption is not reached during the acquisition time, the subtraction of the presumed final value can lead to substantial errors. Although nonlinear fitting of the expression ($a \exp(-t/\tau) + b$) to the data can solve this problem, here we will present an evaluation procedure for this case that is not only much simpler and faster but also much more reliable and accurate. Its most attractive feature is that it is equally applicable if the decay is nonexponential, even if the decay follows an unknown rate law.

Let a species (in our case, the MLCT state) decay by luminescence with an arbitrary rate law, and let this species be the only source of luminescence. Then, the luminescence obeys eq 3. Let the transient absorption be caused by the same process and, in addition, by one or several products X that are formed instantaneously and are stable on the time scale of the luminescence decay. For that situation, the transient absorption is given by

$$\Delta E_\lambda(I_{exc}, t) = \Delta\epsilon_{MLCT,\lambda} \cdot c_{MLCT}(I_{exc}, t) \cdot d + \Delta E_{X,\lambda}(I_{exc}) \quad (4)$$

Eliminating c_{MLCT} from eqs 3 and 4 and rearranging, one gets

$$\Delta E_\lambda(I_{exc}, t) = a \cdot I_{lum,\lambda'}(I_{exc}, t) + \Delta E_{X,\lambda}(I_{exc}) \quad (5)$$

For fixed I_{exc}, this is seen to be a standard linear-regression problem of transient absorption versus luminescence at each point in time, with the scaling factor a and the limiting absorption $\Delta E_{X,\lambda}$ as parameters. However, in a series of otherwise identical measurements with varied I_{exc}, the quantity a must be a global constant. In Appendix I, the equations for such a global linear regression are derived. Because the fit problem is linear, there are no convergence or stability problems whatsoever, as opposed to a nonlinear fit, and the calculation is extremely fast.

The method is even applicable if the absorption of X is not constant, in which case it would yield an average of $\Delta E_{X,\lambda}(I_{exc})$ during the time over which the fit extends. Consequently, discrepancies between the value of $\Delta E_\lambda(I_{exc}, t) - a_{best\ fit} \cdot I_{lum,\lambda'}(I_{exc}, t)$ and the best-fit parameter $\Delta E_{X,\lambda}(I_{exc})$ will reveal any time dependence of the absorption of X. Pertinent plots are given in Figure 6 and show that the limiting absorption is indeed constant on the time scale of the luminescence decay. Because the human eye is extremely sensitive to deviations from a straight line, this is a much more stringent test than that obtainable by an inspection of a nonlinear fit or of the curves of Figure 5.

By carrying out this procedure at different observation wavelengths, one arrives at the spectra of the species responsible for the time-dependent and the time-independent contribution to the transient absorption on the 10-μs time scale. This will be deferred to a later section; as will be shown there, X is the oxidized complex $[Ru(bpy)_3]^{3+}$, and no other ruthenium-based species besides $[Ru(bpy)_3]^{2+}$, $*[Ru(bpy)_3]^{2+}$, and $[Ru(bpy)_3]^{3+}$ is involved in the reaction.

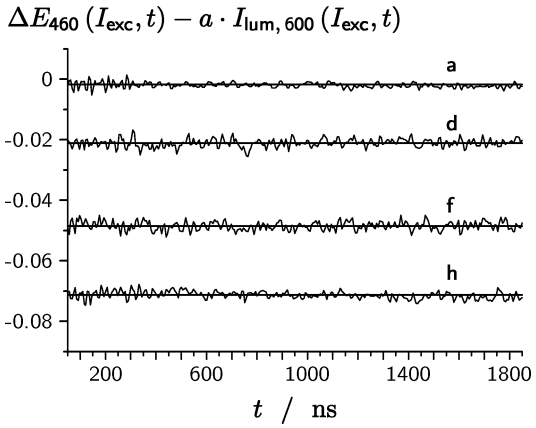

Figure 6. Global fits of eq 5 to traces a, d, f, and h of Figure 5 and the corresponding luminescence decay curves (not shown) with the method given in Appendix I. Fit start, 50 ns after the (negative) rise of the absorption. The straight lines represent the respective values of $E_{X,460}(I_{exc})$. For further explanation, see the text.

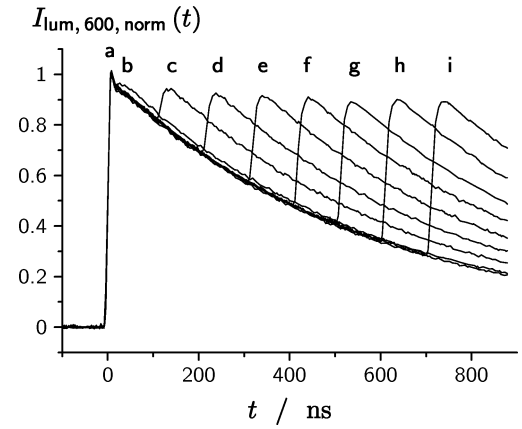

Figure 7. Two-pulse experiments on an N_2O-saturated solution of 3×10^{-5} M $[Ru(bpy)_3]^{2+}$. Shown are the luminescence traces at 600 nm, $I_{lum,600,norm}$, normalized to the inital luminescence at infinite $I_{exc,532}$ (see Figure 3). First pulse: 532 nm, 350 mJ/cm^2, corresponding to conversion of ca. 95% of $[Ru(bpy)_3]^{2+}$ into the MLCT state; second pulse: 308 nm, 90 mJ/cm^2, corresponding to the maximum luminescence obtainable. In trace a, only the 532-nm pulse was applied; in trace b, the 308-nm pulse started immediately after the end of the 532-nm pulse; in traces c to i, the interpulse delay was increased in increments of 100 ns.

Two-Pulse Experiments. By administering a 532-nm pulse of variable intensity before a 308-nm photolysis pulse, any desired concentration ratio of the ground state and the MLCT state can be established before the photoionization. As an expedient variant, which reduces calibration errors, one can employ the 532-nm pulse at fixed intensity and adjust the concentration ratio by the interpulse delay.

Figure 7 shows the outcome of a sequence of such experiments, in which the MLCT luminescence was observed. The luminescence intensity at the end of the second pulse divided by that at the end of the first pulse directly gives the concentration ratio of the MLCT state at these two points in time. It is seen that a decrease of the initial concentration of the MLCT state from about 90% of the substrate concentration to about 25% has a very small effect only (about a 7% decrease) on the luminescence after the photoionization pulse. Hence, the excitation to the MLCT state must be much more efficient than the subsequent photoionization of that state.

As another application, a 532-nm pulse of high intensity provides a convenient analytical tool to measure the concentration of residual $[Ru(bpy)_3]^{2+}$ after a UV photolysis pulse because

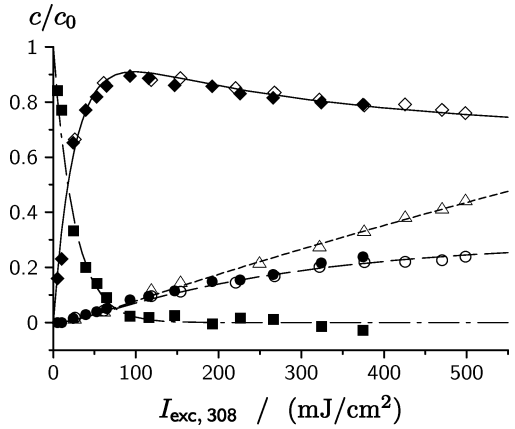

Figure 8. Concentrations c relative to the substrate concentration c_0 as functions of the excitation intensity at 308 nm, $I_{exc,308}$, for a solution of 3×10^{-5} M $[Ru(bpy)_3]^{2+}$, as obtained by two-pulse luminescence experiments (filled symbols) and by single-pulse absorption measurements (open symbols). Squares, ground state; diamonds, MLCT state; circles, oxidized complex; triangles, e_{aq}^-. For further explanation, see the text. All measurements except that of e_{aq}^- were performed in an N_2O-saturated solution. The curves represent a global fit of eqs 16−19 to all data sets simultaneously. Best-fit parameters: $\kappa_1 = 3.94 \times 10^{-2}$ cm²/mJ, $\kappa_2 = 1.09 \times 10^{-3}$ cm²/mJ, $\kappa_3 = 2.56 \times 10^{-3}$ cm²/mJ.

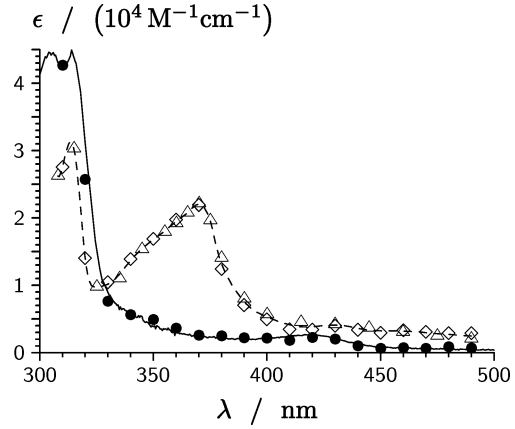

Figure 9. Spectra of the ruthenium-based transients involved in the reaction. Open triangles, absorption spectrum of the MLCT state $*[Ru(bpy)_3]^{2+}$ as obtained by 532-nm excitation and the procedure of Figure 2; the broken line is a spline fit to guide the eye. Solid line, absorption spectrum of the chemically prepared oxidized complex $[Ru(bpy)_3]^{3+}$. Open diamonds and filled circles, spectrum of the time-dependent and the time-independent component of the absorption upon UV irradiation separated by the method of Appendix I.

it quantitatively converts (see Figure 3) the reduced complex $[Ru(bpy)_3]^{2+}$ into the MLCT state but does not respond[3] to the oxidized complex $[Ru(bpy)_3]^{3+}$. By this experiment, in which the 308-nm pulse comes before the 532-nm pulse, one can determine the concentrations of two species (MLCT state and ground state) simultaneously:

Let the luminescence intensity at the end of the 308-nm and the 532-nm pulse be $I_{lum}^{308}(I_{exc,308})$ and $I_{lum}^{532}(I_{exc,308})$; as the notation indicates, *both* signals are functions of the excitation intensity at 308 nm. The concentrations of the MLCT state and residual ground state, $c_{MLCT}(I_{exc,308})$ and $c_{GS}(I_{exc,308})$, are given by

$$\frac{c_{MLCT}}{c_0} = \frac{I_{lum}^{308}(I_{exc,308})}{I_{lum}^{532}(0)} \tag{6}$$

$$\frac{c_{GS}}{c_0} = \frac{I_{lum}^{532}(I_{exc,308}) - I_{lum}^{308}(I_{exc,308})}{I_{lum}^{532}(0)} \tag{7}$$

where c_0 is the substrate concentration.

With the a posteriori knowledge that species X is $[Ru(bpy)_3]^{3+}$ and that the sum of the concentrations of the ground state, MLCT state, and oxidized complex equals c_0, the concentration of the latter species, c_{OX}, can be obtained from

$$\frac{c_{OX}}{c_0} = 1 - \frac{I_{lum}^{532}(I_{exc,308})}{I_{lum}^{532}(0)} \tag{8}$$

whereas the validity of eqs 6 and 7 is not subject to this restriction.

Figure 8 displays the result of a series of such two-pulse experiments, each of which yields the absolute concentrations of all ruthenium-based species at a given intensity of the 308-nm pulse from a single luminescence measurement. As can be seen, the concentration of ground-state molecules becomes negligible at and above the excitation intensity corresponding to the maximum in the MLCT concentration. Also included in the Figure have been the concentrations obtained from single-pulse absorption measurements on the same system. The results with both techniques are seen to agree well, so the two-pulse experiments with luminescence detection provide a complementary approach in situations where absorption measurements should for some reason (e.g., additional absorptions in the presence of other reactants) turn out to be impracticable.

Evaluation of the Absorption Measurements. That the time dependence of the transient absorption on the time scale of up to 10 μs is solely caused by the MLCT state, regardless of whether visible or UV light is used for excitation, is evident from the strict linear relationship between $I_{lum}(t)$ and $\Delta E(t)$. By the same token, the time-dependent components of two transient spectra recorded at different excitation wavelengths can be made to coincide by multiplication with a global factor. Scaling to the substrate concentration (Figure 3) and subtraction of the ground-state spectrum yields the calibrated absorption spectrum of the MLCT state. The spectra in the absence (excitation at 532 nm) and in the presence of photoionization (excitation at 308 or 355 nm) have been superimposed in Figure 9 and are seen to agree very well. There is also good quantitative agreement with the MLCT spectrum determined by three other techniques.[19]

When we varied the excitation intensity at 308 or 355 nm, the absorption spectra remaining after the MLCT state had disappeared were also strictly proportional to one another. Hence, either the long-time component of the transient absorption must be due to a single species, or if this component arises from several species, these must be formed in fixed ratios that are independent of the excitation intensity. Because it is natural to assume that the photoionization of the MLCT state leads to the oxidized ruthenium complex $[Ru(bpy)_3]^{3+}$, we prepared that compound by chemical oxidation of $[Ru(bpy)_3]^{2+}$ and compared the difference spectrum of $[Ru(bpy)_3]^{3+}$ and $[Ru(bpy)_3]^{2+}$ with the time-independent component of our transient spectra. Again, we found a simple proportionality. Figure 9 shows the good agreement between the spectrum of an authentic sample of the oxidized complex and the spectrum obtained from the time-independent component of the transient absorption.

Thus, neither luminescence nor absorption spectra indicate the participation of any ruthenium-based species other than $[Ru(bpy)_3]^{2+}$, $*[Ru(bpy)_3]^{2+}$, and $[Ru(bpy)_3]^{3+}$ in the reaction. This is further corroborated by the results described in the follow-

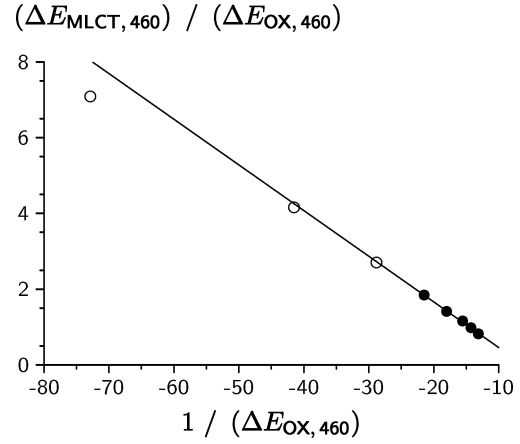

Figure 10. Plot for the determination of the extinction coefficients according to eq 11. For further explanation, see the text. Only those data points depicted as filled circles were included in the regression.

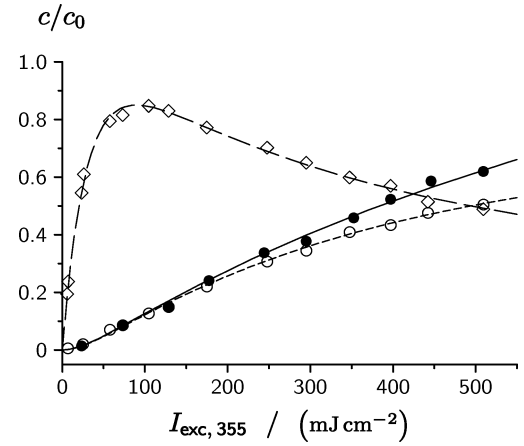

Figure 11. Concentrations c relative to the substrate concentration c_0 as functions of the excitation intensity at 355 nm, $I_{exc,355}$, for a solution of 3×10^{-5} M $[Ru(bpy)_3]^{2+}$ determined by absorption measurements. Open diamonds, MLCT state; open circles, oxidized complex; filled circles, e_{aq}^-. The curves are a global fit of eqs 17−19 to all three data sets simultaneously. Best-fit parameters: $\kappa_1 = 3.51 \times 10^{-2}$ cm²/mJ, $\kappa_2 = 1.88 \times 10^{-3}$ cm²/mJ, $\kappa_3 = 7.85 \times 10^{-4}$ cm²/mJ.

ing: To determine the concentrations from the transient absorption measurements, we must know the extinction coefficients. While they can both be taken from the spectra of Figure 9, their ratio can also be obtained from the transient measurements at 460 nm if the mass balance between the three ruthenium-derived species holds, which, by reverse, provides a test of whether this condition is fulfilled.

The transient absorptions caused by the MLCT state and by the oxidized complex, $\Delta E_{MLCT,\lambda}$ and $\Delta E_{OX,\lambda}$, are related to the concentrations of these species by the difference extinction coefficients, $\Delta\epsilon_{MLCT,\lambda}$ and $\Delta\epsilon_{OX,\lambda}$ (cf. eq 2). This does not imply overall mass balance; the sum of all three concentrations might well be smaller than c_0, but one molecule of $*[Ru(bpy)_3]^{2+}$ or $[Ru(bpy)_3]^{3+}$ formed must mean that one molecule of $[Ru(bpy)_3]^{2+}$ has disappeared.

For the concentrations of $*[Ru(bpy)_3]^{2+}$ and $[Ru(bpy)_3]^{3+}$, one has

$$\frac{c_{OX}}{c_0} \le 1 - \frac{c_{MLCT}}{c_0} \tag{9}$$

At lower excitation intensities, the inequality will certainly apply because there is residual ground-state complex. However, at higher I_{exc}, where there is none (cf. Figure 8), the equality must hold unless the overall mass balance is violated by the formation of additional ruthenium-derived species that were unobservable by our experiments. Inserting the absorbances yields

$$\frac{\Delta E_{OX,\lambda}}{\Delta\epsilon_{OX,\lambda} c_0 d} \le 1 - \frac{\Delta E_{MLCT,\lambda}}{\Delta\epsilon_{MLCT,\lambda} c_0 d} \tag{10}$$

Referring to 460 nm, by multiplying with $\Delta\epsilon_{MLCT,460} c_0 d / (\Delta E_{OX,460})$, which is a positive quantity, and rearranging, one gets

$$\frac{\Delta E_{MLCT,460}}{\Delta E_{OX,460}} \le (\Delta\epsilon_{MLCT,460} c_0 d) \cdot \frac{1}{\Delta E_{OX,460}} - \frac{\Delta\epsilon_{MLCT,460}}{\Delta\epsilon_{OX,460}} \tag{11}$$

A plot of $(\Delta E_{MLCT,460})/(\Delta E_{OX,460})$ as a function of $1/(\Delta E_{OX,460})$ should thus be linear in the range of negligible ground-state concentration provided that the overall mass balance holds. Figure 10 shows that this behavior is indeed realized: at low excitation intensities, there is a distinct curvature of the plot, but at high intensities, good linearity is observed, which means that the system is closed (i.e., that mass balance between the three ruthenium-based species holds).[20]

The slope and intercept of that plot yield the two extinction coefficients needed for evaluation. A comparison with the data of the saturation experiment at 532 nm, Figures 2 and 3, gives very good consistency, the differences between $\Delta\epsilon_{MLCT,460}$ being less than 3%. Determining the extinction coefficients by the same type of experiment as the one they are used to evaluate is not circular but rather has the advantage that any errors in the optical path length (as caused, for example, by a slight overfocusing of the laser) compensate.

Figure 11 shows the intensity dependence, upon 355-nm excitation, of the concentrations obtained from the absorption measurements with these extinction coefficients. The corresponding data for 308-nm excitation have already been included in Figure 8.

The most striking feature in both Figures is the discrepancy between the curves for $[Ru(bpy)_3]^{3+}$ and e_{aq}^-, which is especially pronounced at 308 nm, where the concentration of $[Ru(bpy)_3]^{3+}$ starts to level off at excitation intensities as low as 20% of the maximum whereas the concentration of e_{aq}^- rises undiminishedly. This cannot be due to an experimental artifact, such as an erroneous intensity calibration, a wrong optical path length, or an error in the determination of the extinction coefficient: the first and second would distort both curves horizontally or vertically but would affect both of them in exactly the same way, so their relative appearance would not be changed. The third would cause a vertical scaling of a curve as a whole, so proportional deviations would occur at all intensities, not just at the highest. The observed behavior must thus have a chemical origin.

With a linear photoionization mechanism such as that shown in Scheme 4, the amounts of $[Ru(bpy)_3]^{3+}$ and e_{aq}^- that are formed are necessarily equal. A divergence can be explained only by a more complex reaction mechanism. Moreover, because the deviations are seen to depend on the excitation intensity, their reason must be a secondary photoreaction of $[Ru(bpy)_3]^{3+}$. It is obvious that such effects would have passed unnoticed if detection had been restricted to one species (e.g., the electron).

$[Ru(bpy)_3]^{3+}$ as a Starting Compound. Direct evidence for such a photoreaction of $[Ru(bpy)_3]^{3+}$ is obtained when this compound is prepared by chemical oxidation of $[Ru(bpy)_3]^{2+}$ and subjected to laser flash photolysis under the same conditions as before. As a control experiment, excitation at 532 nm was

first performed on the samples. Neither luminescence nor transient absorption was observed under these conditions, which not only confirms quantitative oxidation (i.e., the absence of residual $[Ru(bpy)_3]^{2+}$) but also indicates that the 532-nm pulse as an analytical tool is not sensitive to $[Ru(bpy)_3]^{3+}$. However, upon a 355-nm or 308-nm pulse, transient signals appear. Their spectra and decay characteristics bear out that they stem from the MLCT state; moreover, after they have decayed completely, they can be recovered quantitatively by a probing 532-nm pulse that had no effect when it was applied on its own or before the UV pulse.[3]

These experiments demonstrate unambiguously that excitation at 355 or 308 nm causes a photoreduction of $[Ru(bpy)_3]^{3+}$.

Two limiting mechanistic scenarios are conceivable for this reaction. It might involve the ground-state complex $[Ru(bpy)_3]^{2+}$ as an intermediate, which is then excited to the MLCT state $*[Ru(bpy)_3]^{2+}$ by the absorption of another photon, or it might lead directly to $*[Ru(bpy)_3]^{2+}$, chemiluminescence being a common phenomenon in other photoreductions of $[Ru(bpy)_3]^{3+}$.[21] The second pathway would provide an alternative explanation of the reported[13] anomalies, if they are genuine effects, of the MLCT luminescence upon high-intensity excitation of $[Ru(bpy)_3]^{2+}$ at 355 nm: A high concentration of $[Ru(bpy)_3]^{3+}$ is present under these conditions (cf. Figure 11), and its photoreduction is significant, as the value of the kinetic constant κ_3 shows (see next section). If that photoreduction, which must be a bimolecular process, is not extremely fast on the time scale of the laser pulse and if it produces the MLCT state, at least partially, some amount of $*[Ru(bpy)_3]^{2+}$ will still be formed after the end of the laser pulse and will cause a rising component of the luminescence. At low $I_{exc,355}$, however, this reaction can be disregarded because the concentration of $[Ru(bpy)_3]^{3+}$ is too small. This effect will be reinforced by the opposite intensity dependence of the MLCT concentration, which peaks at fairly low intensities, where the photoreduction is negligible, and is significantly lower at high intensities, where the photoreduction has its highest turnover.

However tempting this explanation might be, in particular because it is consistent with all of our other results and does not have to invoke species that are, apparently, spectroscopically unobservable, again we have not been able to find unambiguous evidence for a rising component of the luminescence. As in Figure 1, we observed no rise after the overshoot decay (i.e., about 30 ns) in the experiments on $[Ru(bpy)_3]^{3+}$. That the photoreduction is finished on that time scale excludes reactions of two ruthenium-based species at the low concentrations used and leaves a reaction with water as the only possibility. Hence, the mechanism of the photoreduction must differ sharply from that of the thermal reaction, which is slow and thought to involve several molecules of $[Ru(bpy)_3]^{3+}$.[22] This is corroborated by scavenging experiments with benzoic acid, which show[3] that $^{\bullet}OH$ radicals are formed in the photoreduction, which is not observed for the thermal reduction in the homogeneous phase. The photoreduction of $[Ru(bpy)_3]^{3+}$ is thus a photochemically induced water oxidation.

The presence of this reaction makes the overall reaction cyclic. As an attractive feature of this, the electron yield is not limited by the depletion of the ruthenium-based species. Unfortunately, at the available excitation intensities, an electron yield significantly larger than c_0 cannot be achieved with this system owing to unfavorable absorption properties and quantum yields.

As a final test of the mechanism, two experiments were performed under identical conditions except that the starting compound was $[Ru(bpy)_3]^{2+}$ in the first case and $[Ru(bpy)_3]^{3+}$ in the second, and the intensity dependences of the MLCT luminescence were compared. Figure 12 displays the result. The equations derived in the next section can be fitted simultaneously to both data sets and are seen to represent the experimental values quite well (i.e., the curves of both experiments are described by the same kinetic parameters).

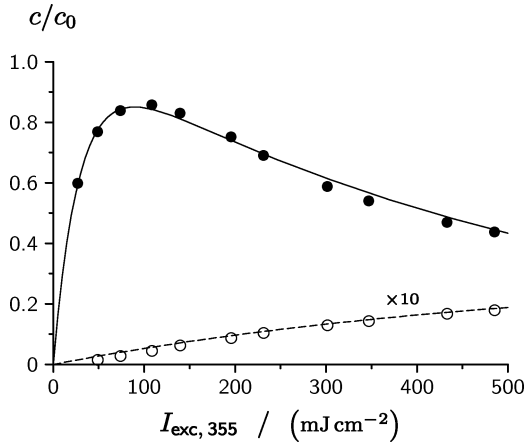

Figure 12. Concentrations c of the MLCT state relative to the substrate concentration c_0 as functions of the excitation intensity at 355 nm, $I_{exc,355}$. Filled circles, reaction starting with $[Ru(bpy)_3]^{2+}$; open circles, starting with the oxidized complex $[Ru(bpy)_3]^{3+}$ at the same concentration, curve multiplied by 10. Experimental conditions: substrate concentration 3×10^{-5} M, pH 0. The curves represent the simultaneous fit of eqs 17 and 20 to the two data sets, with κ_1 and κ_2 kept fixed at the same values as in Figure 11. Best-fit parameter: $\kappa_3 = 5.8 \times 10^{-5}$ cm^2/mJ.

Kinetic Treatment. Because of the low concentrations used and the small optical path length in the direction of the laser beam, our solutions were optically thin with respect to all absorbing species, both at 308 nm and at 355 nm. Therefore, a linearization of the Lambert−Beer law is permissible, and all three steps of the mechanism—excitation of $[Ru(bpy)_3]^{2+}$, ionization of $*[Ru(bpy)_3]^{2+}$, and photoreduction of $[Ru(bpy)_3]^{3+}$—can be described as first-order processes. During the laser pulse, their rate "constants" k_1 to k_3 will vary as the envelope of the pulse; nevertheless, their respective ratios must remain constant because all reactions are driven by the same pulse. Under these circumstances, the actual pulse shape does not play any role, as can also be shown mathematically,[2d] and may be replaced by a rectangle of average intensity I_{exc}/τ, where τ is the pulse duration. Expressing k_i as $\kappa_i I_{exc}/\tau$, with the parameter κ_i having the dimensions of reciprocal intensity, and taking the value at the end of the pulse, one has

$$k_i\tau = \kappa_i I_{exc} \tag{12}$$

The intensity dependence thus follows directly from the integrated rate equations for the kinetic scheme, without any simplifying assumptions.

In our systems, there are only two independent ruthenium-based species because of the mass balance between $[Ru(bpy)_3]^{2+}$, $*[Ru(bpy)_3]^{2+}$, and $[Ru(bpy)_3]^{3+}$. Regardless of the complexity of the mechanism (i.e., of whether the photoreduction of $[Ru(bpy)_3]^{3+}$ leads to the MLCT state (Scheme 5), to the ground state (Scheme 6), or even to a superposition of the two), the intensity dependence of each species is given by a linear combination of the three basis functions

$$\{1, \exp(-\kappa_a I_{exc}), \exp(-\kappa_b I_{exc})\} \tag{13}$$

as can be seen from the theory of coupled sets of first-order

SCHEME 5

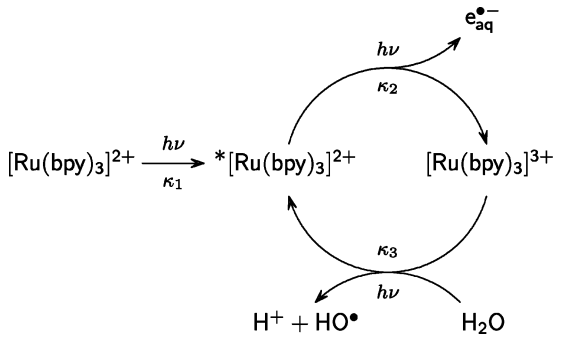

SCHEME 6

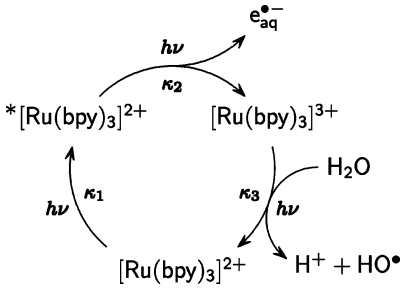

reactions.[23] The two constants κ_a and κ_b are determined by κ_1 to κ_3 in a way specific to the mechanism.

In the simplest case (Scheme 5), one has

$$\kappa_a = \kappa_1 \tag{14}$$

$$\kappa_b = \kappa_2 + \kappa_3 \tag{15}$$

and the closed-form solutions for the reaction starting with $[Ru(bpy)_3]^{2+}$ are

$$\frac{c_{GS}}{c_0} = \exp(-\kappa_a I_{exc}) \tag{16}$$

$$\frac{c_{MLCT}}{c_0} = \frac{\kappa_3}{\kappa_b}\left[1 - \frac{\kappa_b(\kappa_a - \kappa_3)}{\kappa_3(\kappa_a - \kappa_b)}\exp(-\kappa_a I_{exc}) + \frac{\kappa_a(\kappa_b - \kappa_3)}{\kappa_3(\kappa_a - \kappa_b)}\exp(-\kappa_b I_{exc})\right] \tag{17}$$

$$\frac{c_{OX}}{c_0} = \frac{\kappa_2}{\kappa_b}\left[1 + \frac{\kappa_b}{\kappa_a - \kappa_b}\exp(-\kappa_a I_{exc}) - \frac{\kappa_a}{\kappa_a - \kappa_b}\exp(-\kappa_b I_{exc})\right] \tag{18}$$

Although some of the preexponential factors in eqs 16−18 may be simplified, the given forms allow a direct comparison with the solutions for the more complex mechanism of Scheme 6 (see Appendix II).

The concentration of the hydrated electron, c_{el}, follows from the integration of eq 17,

$$\frac{c_{el}}{c_0} = \frac{\kappa_2}{\kappa_b}\left[\frac{\kappa_b(\kappa_a - \kappa_3)}{\kappa_a(\kappa_a - \kappa_b)}\exp(-\kappa_a I_{exc}) - \frac{\kappa_a(\kappa_b - \kappa_3)}{\kappa_b(\kappa_a - \kappa_b)}\exp(-\kappa_b I_{exc}) + 1 - \frac{\kappa_3(\kappa_a + \kappa_b)}{\kappa_a\kappa_b} + \kappa_3 I_{exc}\right] \tag{19}$$

Finally, for the reaction starting with $[Ru(bpy)_3]^{3+}$, the concentration of the MLCT state is calculated to be

$$\frac{c_{MLCT}}{c_0} = \frac{\kappa_3}{\kappa_b}[1 - \exp(-\kappa_b I_{exc})] \tag{20}$$

In Appendix II, closed-form solutions for the mechanism of Scheme 6 are given and compared to the above results. As will be shown there, the two mechanisms are kinetically indistinguishable for the chemical system under study. Although this leaves open the question as to the actual pathway of the photoreduction, by reversing the argument the three kinetic constants κ_1 to κ_3 can be extracted reliably from the intensity-dependent measurements without knowledge of that mechanistic detail. We therefore used eqs 14−20 for evaluation.

Because we measured the intensity dependences of more than one species in parallel, global fits to corresponding data sets can be performed, through which a very low margin of uncertainty is achieved: With three adjustable parameters only, κ_1 to κ_3, three or four curves differing considerably in shape—at 308 nm for all species (Figure 8) and, moreover, obtained by two complementary methods for $[Ru(bpy)_3]^{2+}$ and $[Ru(bpy)_3]^{3+}$ and at 355 nm for $*[Ru(bpy)_3]^{2+}$, $[Ru(bpy)_3]^{3+}$, and $e^{\bullet-}_{aq}$ (Figure 11)—can be fitted simultaneously. The success of these global fits would have established a cyclic mechanism even if it had not been possible to produce direct evidence for the photoreduction of $[Ru(bpy)_3]^{3+}$. Only minute improvements in the fits resulted when the extinction coefficients were tentatively treated as free parameters, so we left them at the values determined independently by the procedure described above; the good consistency indicates the validity of that procedure.

The relationship between a kinetic constant obtained at a particular wavelength, $\kappa_{i,\lambda}$, and the quantum yield, $\phi_{i,\lambda}$, of the corresponding process is given by[2d]

$$\kappa_{i,\lambda} = \frac{2.303\lambda}{hcN_A} \cdot \epsilon_{i,\lambda} \cdot \phi_{i,\lambda} \tag{21}$$

where the first factor depends only on the excitation wavelength and the usual fundamental constants and $\epsilon_{i,\lambda}$ is the extinction coefficient of the pertinent reactant. Reliable measurements of the *absolute* excitation intensity entering the samples are very difficult to perform, especially because of the dissimilar beam characteristics of the 308-nm and the 355/532-nm laser. Also, inner filter effects can play different roles at different excitation wavelengths. It is thus not surprising that the best-fit parameters $\kappa_{1,\lambda}$ deviate from the values calculated by eq 21 with a quantum yield of unity[18,24] for the excitation of $[Ru(bpy)_3]^{2+}$. The experimental constants are always smaller than the theoretical estimates: at 532 nm, the discrepancy is only 3% (Figure 3); at 355 nm, it increases to 11% (Figure 11); and at 308 nm, it becomes as high as 54% (Figure 8).

However, *relative* values of I_{exc} can be determined accurately, so the excitation of $[Ru(bpy)_3]^{2+}$ can be used as an in situ chemical actinometer according to

$$\phi_{i,\lambda} = \frac{\kappa_{i,\lambda}}{\kappa_{1,\lambda}} \cdot \frac{\epsilon_{1,\lambda}}{\epsilon_{i,\lambda}} \tag{22}$$

With eq 22 and the values of κ_2 given in Figures 8 and 11, the quantum yield of photoionization of the MLCT state is found to be 0.016 ± 0.001, independent of the excitation wavelength. This is an order of magnitude higher than previously thought.[10]

Influence of the Reaction Conditions on the Kinetic Parameters. Surprisingly, the photoreduction of $[Ru(bpy)_3]^{3+}$ appears to have a higher quantum yield at 355 nm (0.023) compared to that at 308 nm (0.010). Although no definite conclusion can be drawn from that seeming paradox, it might be consistent with a delayed generation of $*[Ru(bpy)_3]^{2+}$ from photoexcited $[Ru(bpy)_3]^{3+}$, which would also explain the reported[13] fast-rising component of the luminescence after the end of a 355-nm pulse: It is obvious that such a process would manifest itself exactly in that way in the luminescence traces. Because the laser pulse has a finite duration, a short time lag between the excitation of $[Ru(bpy)_3]^{3+}$ and the production of $*[Ru(bpy)_3]^{2+}$ would introduce a small bias to the photostationary state and to the way that state is reached. The amount of $*[Ru(bpy)_3]^{2+}$ observed in our experiments would be slightly increased whereas that of $[Ru(bpy)_3]^{3+}$ would be slightly decreased, which would result in an apparently higher best-fit value of κ_3. The effect would be more pronounced with the shorter 355-nm pulse (8ns) than with the much longer 308-nm pulse (30 ns) (i.e., a higher value of κ_3 would be found at 355 nm than at 308 nm). Although this process would modify the intensity dependences in a nonlinear way, we have recently shown[2d] for a simpler cyclic photoreaction that such deviations are small provided that the lag is not longer than the pulse. Because our experiments (Figure 1) indicate a considerably shorter lag than 27 ns, it is not unreasonable to assume that the effect is kinetically unobservable in the intensity dependences.

The comparison of $[Ru(bpy)_3]^{2+}$ and $[Ru(bpy)_3]^{3+}$ as starting materials (Figure 12) reveals another interesting facet of that photoreduction. To ensure sufficient stability of the chemically generated oxidized complex, these measurements had to be carried out at pH 0, as opposed to all the previous ones (pH 7 or above). The absorption spectrum of $[Ru(bpy)_3]^{2+}$ is independent of pH and the influence of protons on the efficiency of intersystem crossing to the MLCT state is hardly conceivable, so we kept the parameter κ_1 fixed at the best-fit value found before. Both κ_2 and κ_3 were initially treated as a free parameters. However, the simultaneous fit of eqs 17 and 20 to the two data sets converged on a best-fit value of κ_2 that differed from the one at pH 7 by less than 4%. We took this to indicate that κ_2 is also independent of pH and froze it at the result for pH 7 (which is also found at higher pH). A very good fit to both data sets is obtained with κ_3 as the only adjustable kinetic constant, as the Figure shows. From pH 7 to 0, κ_3 is seen to decrease by a factor of 13.5.

Conclusions

All of these results shed new light on a long-known[10,11] photoreaction—the photoionization of $[Ru(bpy)_3]^{2+}$—and demonstrate the pivotal role of the previously unrecognized photoreduction of $[Ru(bpy)_3]^{3+}$ in the reaction mechanism. The inclusion of that step might also modify the reported[11,12] influence of SDS on the photoionization efficiency. Further work focusing on these aspects is in progress.

Appendix I

Let there be a total of n pairs of sets of discrete data, f_{ij} and g_{ij}, among which a linear relationship is expected to hold

$$f_{ij} = a \cdot g_{ij} + b_i \tag{23}$$

with a factor a common to all pairs but with the additive term b_i different for each pair. Let the index i denote the pair ($1 \le i \le n$), and let the two data sets of each pair be of equal length l_i; let the index j denote a particular data element ($1 \le j \le l_i$).

To determine the best-fit parameters a and $b_1 \ldots b_n$, the sum of squared deviations

$$\sum_i^n \sum_j^{l_i} (f_{ij} - a \cdot g_{ij} - b_i)^2 \tag{24}$$

has to be minimized with respect to each parameter.

Differentiating eq 24 with respect to a, setting the result equal to zero, canceling multiplicative constants, and rearranging, one gets

$$a \sum_i^n \sum_j^{l_i} g_{ij}^2 + \sum_i^n \left(b_i \sum_j^{l_1} g_{ij} \right) = \sum_i^n \sum_j^{l_i} f_{ij} g_{ij} \tag{25}$$

For each parameter b_i, the same procedure yields

$$a \sum_j^{l_i} g_{ij} + b_i l_i = \sum_j^{l_i} f_{ij} \tag{26}$$

The matrix of coefficients of the system of linear equations given by eqs 25 and 26 is thus symmetric and composed of a diagonal matrix diag($l_1, \ldots, l_n$) flanked by

$$\left(\sum_i^n \sum_j^{l_i} g_{ij}^2, \sum_j^{l_1} g_{1j}, \ldots, \sum_j^{l_n} g_{nj} \right)$$

as the first row or column. By iterative expansion, one can show that its determinant has the value q,

$$q = \left(\prod_k^n l_k \right) \left(\sum_i^n \sum_j^{l_i} g_{ij}^2 \right) - \sum_i^n \left[\left(\prod_{k \ne i}^n l_k \right) \left(\sum_j^{l_i} g_{ij} \right)^2 \right] \tag{27}$$

In the same way, one gets the value p of the determinant that results when the first column of the determinant of coefficients is replaced by the right-hand side of eqs 25 and 26

$$p = \left(\prod_k^n l_k \right) \left(\sum_i^n \sum_j^{l_i} f_{ij} g_{ij} \right) - \sum_i^n \left[\left(\prod_{k \ne i}^n l_k \right) \left(\sum_j^{l_i} f_{ij} \right) \left(\sum_j^{l_i} g_{ij} \right) \right] \tag{28}$$

Once the best-fit parameter a has been obtained by

$$a = \frac{p}{q} \tag{29}$$

the other parameters b_i follow by a straightforward insertion of its value into eq 26. The result is

$$b_i = \frac{1}{l_i} \left(\sum_j^{l_j} f_{ij} - \left(\frac{p}{q} \right) \sum_j^{l_j} g_{ij} \right) \tag{30}$$

The expressions and the calculation procedure are simplified considerably if all data sets have the same length l. Under these circumstances, only one pair of data sets has to be kept in core memory at a time and yields increments p_i and q_i:

$$p_i = l \sum_j^l f_{ij} g_{ij} - \left(\sum_j^l f_{ij} \right) \left(\sum_j^l g_{ij} \right) \tag{31}$$

$$q_i = l \sum_j^l g_{ij}^2 - \left(\sum_j^l g_{ij} \right)^2 \tag{32}$$

By successively summing up all of these increments, one obtains p and q,

$$p = \sum_i p_i \tag{33}$$

$$q = \sum_i q_i \tag{34}$$

Appendix II

For the mechanism of Scheme 6, the two characteristic constants κ_a and κ_b are given by

$$\kappa_{a,b} = \frac{1}{2}\left[\kappa_1 + \kappa_2 + \kappa_3 \pm \sqrt{(\kappa_1 + \kappa_2 + \kappa_3)^2 - 4(\kappa_1\kappa_2 + \kappa_1\kappa_3 + \kappa_2\kappa_3)}\right] \tag{35}$$

By putting κ_1, which will always be considerably larger than κ_2 and κ_3, outside the brackets and expanding the square root to second order in the ratios of constants, one finds

$$\kappa_a \approx \kappa_1[1 - (\kappa_2/\kappa_1) \cdot (\kappa_3/\kappa_1)] \tag{36}$$

$$\kappa_b \approx (\kappa_2 + \kappa_3)\left[1 + \frac{(\kappa_2/\kappa_1) \cdot (\kappa_3/\kappa_1)}{(\kappa_2/\kappa_1) + (\kappa_3/\kappa_1)}\right] \tag{37}$$

Equation 36 shows that κ_a deviates from κ_1 in second- and higher-order terms only.

When only ground-state molecules are present before the laser pulse, the closed-form solutions for the concentrations after the pulse are found to be

$$\frac{c_{GS}}{c_0} = \frac{\kappa_1}{\kappa_a}\left[\frac{\kappa_2\kappa_3}{\kappa_1\kappa_b} + \frac{\kappa_a - (\kappa_2 + \kappa_3)}{\kappa_a - \kappa_b}\exp(-\kappa_a I_{exc}) - \frac{\kappa_a}{\kappa_b} \cdot \frac{\kappa_b - (\kappa_2 + \kappa_3)}{\kappa_a - \kappa_b}\exp(-\kappa_b I_{exc})\right] \tag{38}$$

$$\frac{c_{MLCT}}{c_0} = \frac{\kappa_1}{\kappa_a}\left\{\frac{\kappa_3}{\kappa_b}\left[1 - \frac{\kappa_b(\kappa_a - \kappa_3)}{\kappa_3(\kappa_a - \kappa_b)}\exp(-\kappa_a I_{exc}) + \frac{\kappa_a(\kappa_b - \kappa_3)}{\kappa_3(\kappa_a - \kappa_b)}\exp(-\kappa_b I_{exc})\right]\right\} \tag{39}$$

$$\frac{c_{OX}}{c_0} = \frac{\kappa_1}{\kappa_a}\left\{\frac{\kappa_2}{\kappa_b}\left[1 + \frac{\kappa_b}{\kappa_a - \kappa_b}\exp(-\kappa_a I_{exc}) - \frac{\kappa_a}{\kappa_a - \kappa_b}\exp(-\kappa_b I_{exc})\right]\right\} \tag{40}$$

where we have chosen such forms of the preexponential factors as to allow a direct comparison with the results for the mechanism of Scheme 5. The expressions inside the curly brackets of eqs 39 and of 40 are seen to be identical to eqs 17 and 18. Hence, in the reaction starting with $[Ru(bpy)_3]^{2+}$, the curves for the MLCT state and the oxidized complex do not allow a distinction: They have exactly the same functional form in both cases, the only difference with the mechanism of Scheme 6 being a scaling of both curves by the factor κ_1/κ_a, which up to second order is $1 + (\kappa_2/\kappa_1) \cdot (\kappa_3/\kappa_1)$. For the kinetic parameters extracted from Figures 8 and 11, this deviates from unity by less than 0.2% and is thus utterly undetectable by the measurements. The same holds for the electron curve because it follows from an integration of the curve for the MLCT state, eq 39 or 17, respectively.

In principle, the curve for the ground state is better suited for a distinction because an additional exponential term and an additional constant term appear with the mechanism of Scheme 6. However, on the basis of the experimentally obtained parameters, the constant term is calculated to be less than 2% of c_0, and the same factor enters the amplitude of the second exponential in Eq 38. Hence, for our systems, the effect is too small to permit a reliable kinetic differentiation between Scheme 5 and 6. The situation is similar when $[Ru(bpy)_3]^{3+}$ is the starting material: In contrast to eq 20, an induction period must result if the photoreduction of $[Ru(bpy)_3]^{3+}$ leads to a ground-state molecule; numerically, however, this effect is again very small.

It is obvious that a superposition of the two mechanisms will yield a result that lies between the two limiting cases discussed; a separation of both pathways, if both of them are taken, would thus be even more difficult.

References and Notes

(1) (a) McGimpsey, W. G. *Trends Org. Chem.* **1997**, *6*, 233−257. (b) McGimpsey, W. G. *Mol. Supramol. Chem.* **1998**, *2*, 249−306. and references therein.

(2) (a) Goez, M.; Zubarev, V. *Angew. Chem., Int. Ed. Engl.* **1997**, *36*, 2664−2666. (b) Goez, M.; Zubarev, V.; Eckert, G. *J. Am. Chem. Soc.* **1998**, *120*, 5347−5348. (c) Goez, M.; Zubarev, V. *J. Phys. Chem. A* **1999**, *103*, 9605−9613. (d) Goez, M.; Zubarev, V. *Chem. Phys.* **2000**, *256*, 107−116.

(3) Goez, M.; Schiewek, M.; Musa, M. H. O. *Angew. Chem., Int. Ed.* **2002**, *41*, 1535−1538.

(4) Goez, M.; Hussein, B. H. M. *Angew. Chem., Int. Ed.* **2003**, *42*, 1659−1661.

(5) Goez, M.; Zubarev, V. *Angew. Chem., Int. Ed.* **2001**, *40*, 2867−2869.

(6) Braterman, P. S.; Harriman, A.; Heath, G. A.; Yellowlees, L. J. *J. Chem. Soc., Dalton Trans.* **1983**, 1801−1803.

(7) Spinks, J. W. T.; Woods, R. J. *An Introduction to Radiation Chemistry*; Wiley: New York, 1976.

(8) Balzani, V.; Barigelletti, F.; DeCola, L. *Top. Curr. Chem.* **1990**, *158*, 31−71.

(9) Roundhill, D. M. Photochemistry and Photophysics of Metal Complexes. In *Modern Inorganic Chemistry*; Fackler, J. P., Ed.; Plenum Press: New York, 1994.

(10) Meisel, D.; Matheson, M. S.; Mulac, W. A.; Rabani, J. *J. Phys. Chem.* **1977**, *81*, 1449−1455.

(11) Atherton, S. J. *J. Phys. Chem.* **1984**, *88*, 2841−2844.

(12) (a) Naik, D. B.; Schnabel, W. *Chem. Phys. Lett.* **1994**, *228*, 616−620. (b) Naik, D. B.; Schnabel, W. *Chem. Phys. Lett.* **1999**, *315*, 416−420.

(13) Thompson, D. W.; Wishart, J. F.; Brunschwig, B. S.; Sutin, N. *J. Phys. Chem. A* **2001**, *105*, 8117−8122.

(14) Creutz, C.; Sutin, N. *Proc. Natl. Acad. Sci. U.S.A.* **1975**, *72*, 2858−2862.

(15) (a) Van Houten, J.; Watts, R. J. *J. Am. Chem. Soc.* **1976**, *98*, 4853−4858. (b) Van Houten, J.; Watts, R. J. *Inorg. Chem.* **1978**, *17*, 3381−3385.

(16) Durham, B.; Caspar, J. V.; Nagle, J. K.; Meyer, T. J. *J. Am. Chem. Soc.* **1982**, *104*, 4803−4810.

(17) We chose this particular wavelength because it corresponds to a pronounced peak in the emission spectrum of the monitoring high-pressure xenon lamp. The photon flux at 830 nm is an order of magnitude higher than in the range from 500 to 850 nm, with concomitant gain in the signal-to-noise ratio.

(18) Shimizu, O.; Watanabe, J.; Naito, S. *Chem. Phys. Lett.* **2000**, *332*, 295−298.

(19) Yoshimura, A.; Hoffman, M. Z.; Sun, H. *J. Photochem. Photobiol., A* **1993**, *70*, 29−33.

(20) A nonzero ground-state concentration $c_{GS,\infty}$ remaining at infinite excitation intensity, as would result from Scheme 6, would not destroy linearity but merely cause the slope to be multiplied by $(1 - c_{GS,\infty}/c_0)$.

(21) Gerardi, R. D.; Barnett, N. W.; Lewis, S. W. *Anal. Chim. Acta* **1999**, *378*, 1−43.

(22) Ghosh, P. K.; Brunschwig, B. S.; Chou, M.; Creutz, C.; Sutin, N. *J. Am. Chem. Soc.* **1984**, *106*, 4772−4783.

(23) Matsen, F. A.; Franklin, J. L. *J. Am. Chem. Soc.* **1950**, *72*, 3337−3341.

(24) (a) Demas, J. N.; Taylor, D. G. *Inorg. Chem.* **1979**, *18*, 3177−3179. (b) Bolletta, F.; Juris, A.; Maestri, M.; Sandrini, D. *Inorg. Chim. Acta* **1980**, *44*, L175−L176.